Laser and Particle Beams (2017), *35*, 64–71.

doi:10.1017/S0263034616000823

The combination of cold and hot components in the energy spectra of electrons scattered by relativistically intense laser pulses with various transverse distributions of amplitude

O.B. SHIRYAEV[1,2]

[1]Department of Coherent and Nonlinear Optics, General Physics Institute of the Russian Academy of Science, 38 Vavilov Street, Box 117942, Moscow, Russia
[2]Medicobiologic Faculty, N.I. Pirogov Russian National Research Medical University, 1 Ostrovitianov Street, Box 117997, Moscow, Russia

(Received 2 October 2016; Accepted 12 November 2016)

Abstract

The energy spectra of a sparse ensemble of electrons scattered by relativistically intense laser pulses are studied numerically by solving the relativistic Newton equations with the Lorentz force generated by an electromagnetic envelope in vacuum. The expressions for the envelope describe focused optical fields, include significant short-pulse corrections, and afford the representation of laser radiation with various types of transverse distributions of amplitude. The dependence of the character of the electron energy spectra on the type of the transverse distribution of laser amplitude is explored. For Gaussian pulses, the electron energy spectra within specific angular ranges tend to either include a relativistic maximum while being localized around it or to have the shapes of evanescent distributions dominated by the cold component. Conversely, the energy spectra of electrons ejected into certain angular ranges by laser pulses having first-order Laguerre profiles combine pronounced cold components and structured strongly relativistic features. The presumed laser pulse transverse structure and the shapes of the calculated electron energy spectra for first-order Laguerre amplitude distributions are shown to match, qualitatively, those reported in a recent experimental study by Kalashnikov *et al*. in 2015, which revealed the electron energy spectra spanning both the sub-relativistic and the markedly relativistic energy domains.

Keywords: Electron acceleration; Electron energy spectra; Relativistic intensity

1. INTRODUCTION

The interactions between relativistically intense laser pulses and matter are a central theme in modern laser and plasma physics (Mourou *et al.*, 2006; Norreys *et al.*, 2009). The relativistic diapason of intensities, which corresponds to the optical field strengths inducing relativistic dynamics of laser-driven electrons, stretches beyond the threshold value defined as

$$I_r = \frac{m^2 c^3 \omega^2}{8\pi e^2}. \quad (1)$$

Here m and e are the electron mass and charge magnitude, and ω is the field oscillation frequency. For laser wavelength λ, the relativistic intensity makes $1.37 \times 10^{18}\ (1/\lambda[\mu m])^2$ W/cm^2. Currently, laser systems in a number of laboratories worldwide output femtosecond pulses with intensities exceeding the above value by orders of magnitude [considerable potential exists for transcending the current laser intensity limits with the help of sophisticated laser–matter interaction arrangements (Bulanov *et al.*, 2013)].

Laser physics at relativistic intensities promises a series of novel applications, particularly, in the sphere of the acceleration of charged particles. The energy spectra of electrons accelerated at various angles to the optical field propagation axis by laser irradiation of a sparse target are studied in the present paper in the wake of a recent experimental inquiry (Kalashnikov *et al.*, 2015).

The schemes of accelerating electrons with the help of extremely intense laser radiation rely either on the conversion of electromagnetic field energy in plasmas via wakefields (Mori, 2007; Esarey *et al.*, 2009; Malka, 2012) and wave

Address correspondence and reprint requests to: O.B. Shiryaev, Department of Coherent and Nonlinear Optics, General Physics Institute of the Russian Academy of Science, 38 Vavilov Street, Box 117942, Moscow, Russia. E-mail: shiryaev@kapella.gpi.ru

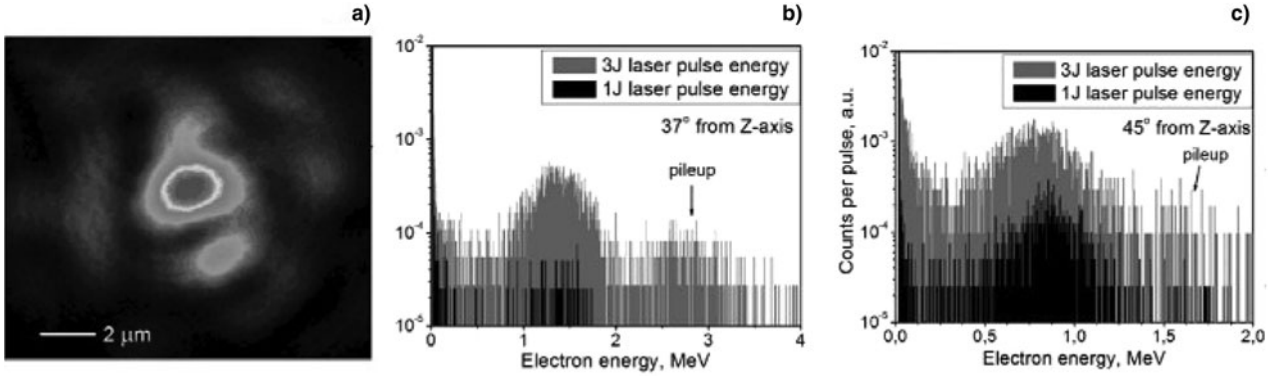

Fig. 1. The experimental results on the interactions between relativistically intense ($I > 10^{20}$ W/cm^2) ultrashort (~30 fs) laser pulses and low-density (3×10^{-4} mbar pressure) Ar targets (Kalashnikov *et al.*, 2015): (a) Distribution of the laser intensity at the beam waist [Fig. 1a from the study by Kalashnikov *et al.* (2015)]; (b, c) Electron energy spectra in the plane of laser pulse polarization sampled at different angles to the propagation axis [Figs. 2a and 2b from the study by Kalashnikov *et al.*, (2015)]. The electron energy data in the study were accumulated over 10,000 shots and statistically processed to introduce adjustments for detector efficiency.

breaking (Ohkubo, 2006) or on the direct driving of electrons in vacuum by the focused envelope optical field (Wang *et al.*, 1998). Note that the acceleration of electrons by intense laser pulses focused into spots of the order of a single wavelength is also being explored (Bochkarev & Bychenkov, 2007). In practice, the direct driving approach is implemented in the form of accelerating bunches of electrons with densities low enough to neglect the Coulomb interactions within them. The optical field for the purpose can be produced by a single laser pulse (Kong *et al.*, 2000; Wang *et al.*, 2001, 2002; Cao *et al.*, 2002; Pang *et al.*, 2002; Salamin *et al.*, 2002; Galkin *et al.*, 2008; Payeur, 2012) or, as proposed in recent studies, by the interference of several tailored laser pulses (Galkin *et al.*, 2012; Korobkin *et al.*, 2013).

The dynamics of an individual electron in a relativistically intense laser envelope has been explored to an extent, the key regime including the capture of the electron by the field, a period of acceleration and dephasing, and the release of the charged particle with substantial residual energy. Accordingly, the simulations of the electron motions employ a theory of focused electromagnetic field in vacuum, which was originally derived by Quesnel and Mora (1998) in the form of an asymptotic expansion of a solution to the Maxwell equations in a small parameter proportional to the ratio of the laser wavelength to the focal spot radius. The series comprise terms with alternate powers of the small parameter, while the temporal profile of the laser pulse is described as a parametric dependence built into this asymptotic expansion (Quesnel & Mora, 1998). As shown below, such framework requires refinement for short laser pulses.

Calculations of the energy spectra integrated over all angles are available (Cao *et al.*, 2002; Cao *et al.*, 2004; Galkin *et al.*, 2010) [angular spectra integrated over energies are also calculated (Cao *et al.*, 2004)] and, moreover, the slope of the resulting distribution has been linked to the incident laser intensity in the case of a Gaussian pulse (Galkin *et al.*, 2010).

A probe into the aspect of optimizing the electron injection conditions for laser acceleration, assuming a focused Gaussian laser pulse shape, showed that the electron energy gains are highly sensitive to the combinations of injection energies and momenta (Zheng *et al.*, 2008). A sketchy relation between the energies and ejection angles of laser-driven electrons was suggested on the basis of the theory of electron dynamics in the field of a plane wave (Hartemann *et al.*, 1998), but the underlying assumptions need to be reconciled with the situation of focused laser pulses [some of the available simulations appear to demonstrate the possibility of departures from the above energy-angle dependence (Cao *et al.*, 2004)].

A recent experimental study of the scattering of low-density targets by laser pulses having the peak intensity of the order of 10^{20} W/cm^2 and the duration of about 30 fs (Kalashnikov *et al.*, 2015) revealed extremely extended post-interaction electron energy spectra, in which energies ranging from the sub-relativistic to the markedly relativistic magnitudes were found to be bracketed together at some of the observation angles. Furthermore, the data include a photograph of the laser beam focus with legible signs of the presence of a ring-shaped structure around the brighter core (Kalashnikov *et al.*, 2015), inviting the hypothesis about the first-order Laguerre transverse distribution of the optical field amplitude. The pertinent results obtained by Kalashnikov *et al.* (2015) are reproduced in Figure 1.

An effort to simulate the electron scattering under the experimental conditions of the above inquiry had been made (Borovskiy *et al.*, 2015), but, contrary to the experimental indications seen in Figure 1a, the modeling by Borovskiy *et al.* (2015) was performed presuming the Gaussian transverse shape of the optical pulses. It is also essential that these simulations were carried out using a model shown below to lack the necessary short-pulse corrections. Ultimately, the simulations by Borovskiy *et al.* (2015) did not reproduce the near-exponential cold parts of the electron energy spectra, which had been a key finding of the experimental study.

https://doi.org/10.1017/S0263034616000823 Published online by Cambridge University Press

In the present paper, the numerical part of the analysis, which is conducted in the framework of a new general model, is largely geared toward providing a theoretical groundwork for the aforementioned experimental results reported by Kalashnikov *et al.* (2015).

The simulations detailed below demonstrate that the character of the registered spectra spanning both cold and detached relativistic energy zones can be traced back to the mingling scattering action of the stronger field at the center and the less intense field at the periphery of pulses having Laguerre transverse profiles.

In this paper, a comprehensive model is laid out on the basis of Maxwell equations for a focused electromagnetic envelope propagating in vacuum. The formulation includes the longitudinal component of the laser field along with the high-order correction due to short-pulse effects. The duration-related correction is comparable in magnitude to the longitudinal field but is missing in previously reported numerical studies, which do take the longitudinal field into account. The model employed here covers optical pulses having the structure of a superposition of Laguerre modes. The electron energy spectra are computed below for several angular ranges for a target sparse enough to neglect the Coulomb interactions within it, specifically assuming a perfectly Gaussian and a first-order Laguerre laser pulse transverse amplitude distribution. The objective is to identify the resulting patterns and to assess the impact of the structure of the transverse distribution of the optical field on the energy spectra of laser-accelerated electrons at relativistic intensities. Overall, the simulations performed below assuming a Laguerre profile of the optical field lead to results which agree, on the qualitative level, with the experimental findings of Kalashnikov *et al.* (2015).

2. FOCUSED OPTICAL FIELD MODEL WITH LONGITUDINAL-FIELD AND SHORT-PULSE CORRECTIONS

Consider the Maxwell equations (Coulomb gauge) for the laser pulse vector potential in vacuum

$$\Delta \mathbf{A} - \partial_t^2 \mathbf{A} = 0, \quad (\nabla, \mathbf{A}) = 0, \tag{2}$$

where $\nabla = (\partial_x, \partial_y, \partial_z)$. The coordinates and time in Eq. (2) are normalized by w_0 and w_0/c, c standing for the speed of light and w_0 being a parameter to be ultimately equated to the focused laser pulse waist. The vector potential in Eq. (2) is normalized by mc^2/e. Assuming that the electromagnetic field is a linearly polarized envelope such that $A_y \equiv 0$, we seek solutions to Eq. (2) of the form

$$A_x = \exp\Big(i\frac{t-z}{\epsilon}\Big)\Big(a(\tau, x, y, s) + \sum_{m=1}^{\infty} \epsilon^m a_{x,m}(\tau, x, y, s)\Big) + \text{c.c.}, \tag{3}$$

$$A_z = \exp\Big(i\frac{t-z}{\epsilon}\Big)\sum_{m=1}^{\infty} \epsilon^m a_{z,m}(\tau, x, y, s) + \text{c.c.}, \tag{4}$$

with $\tau = 2\epsilon z$, $s = t - z$, and $\epsilon = (\lambda/2\pi w_0)$, where λ is the laser pulse wavelength. In line with the envelope approximation, ϵ is assumed to be a small parameter. The lowest and first-order results derived by substituting Eqs. (3) and (4) into the first of Eq. (2) are Schröedinger equations for the corresponding envelopes

$$4i\partial_\tau a + \triangle_\perp a = 0, \tag{5}$$

$$-4i\partial_\tau a_{x,1} + \triangle_\perp a_{x,1} = 4\partial_{\tau s}^2 a \tag{6}$$

with $\Delta_\perp = \partial_x^2 + \partial_y^2$. Solutions to Eqs. (5) and (6), along with the expression for the first-order envelope defined by Eq. (4), are easily found to be of the form

$$a(\tau, x, y, s) = a_0(s)u(\tau, x, y), \tag{7}$$

$$a_{x,1}(\tau, x, y, s) = ia_0'(s)\partial_\tau\big(\tau u(\tau, x, y)\big), \tag{8}$$

$$a_{z,1}(\tau, x, y, s) = -ia_0(s)\partial_x u(\tau, x, y), \tag{9}$$

where $u(\tau, x, y)$ is a solution to Eq. (5). Importantly, the term given by Eq. (8) provides a first-order correction within the overall expression (3), which governs the transverse field. This correction is duration-related, is of the same magnitude as the longitudinal field, and should be taken into account for short laser pulses. Obviously, the duration-related correction vanishes in the long-pulse limit, in which the above model reverts to the one used previously by Galkin *et al.* (2008).

The solution which resulted from earlier derivations (Quesnel and Mora, 1998; Salamin *et al.*, 2002) aimed at describing the transverse component of the vacuum optical field was developed under the *a priori* assumption that it can be represented asymptotically as a sum of terms proportional to even powers of the small parameter and, hence, ignored the short-pulse effects.

In the case of axial symmetry, the simplest case is embodied in the solution of the form

$$u(\tau, x, y) = \frac{\Lambda(\tau, r)}{\sqrt{\tau^2+1}}\exp\big(i\psi(\tau, r)\big),$$

$$\Lambda(\tau, r) = \exp\Big(-\frac{r^2}{\tau^2+1}\Big), \quad \psi(\tau, r) = -\frac{\tau r^2}{\tau^2+1} + \arctan(\tau).$$

Laguerre beams are a more general example of solutions to Eq. (5)

$$u(\tau, x, y) = \frac{2^{l/2}\big(\big[r/(\sqrt{\tau^2+1})\big]\big)^l \sin\big(l\varphi + \varphi_0\big)L_\delta^l\big(\big[2r^2/(\tau^2+1)\big]\big) \times \exp\big(i(2\delta + l + 1)\tan^{-1}(\tau) - \big(\big[r^2(1+i\tau)\big]/[\tau^2+1]\big)\big)}{\sqrt{\tau^2+1}}. \tag{10}$$

https://doi.org/10.1017/S0263034616000823 Published online by Cambridge University Press

Here $\varphi = \arctan(y/x)$ and φ_0 is an integration constant. A superposition of Laguerre modes constitutes the general solution describing a focused optical field in vacuum. The above Laguerre mode is reduced to a Gaussian one when $l = 0$ and $\delta = 0$.

Altogether, Eqs. (3), (4) and (7)–(10) define the lowest and first-order approximations to a solution to the Maxwell equations governing the propagation of a short, focused electromagnetic envelope in vacuum. The approach can be extended to obtain higher approximations, but the corrections are unlikely to contribute substantially to the electron dynamics for a realistic combination of the values of laser wavelength and beam waist.

It should be noted that efforts have been made to study charged particle acceleration by optical fields with structures more complex than Gaussian pulses. Vacuum acceleration by Airy beams (Li *et al.*, 2010) and by Gaussian modes (Wang *et al.*, 2007) was examined. The issue of high-order corrections to the expressions for the field of an ultrashort laser pulse in vacuum was also addressed (Hua *et al.*, 2004).

The electromagnetic field being defined by Eqs. (3), (4) and (7)–(9), the relativistic Newton equation for an electron driven by the corresponding Lorentz force is

$$\mathbf{p}_t = -\left(\mathbf{E} + \gamma^{-1}\mathbf{p} \times \mathbf{H}\right), \tag{11}$$

the electron momentum being normalized by mc. Here $\mathbf{E} = -\partial_t \mathbf{A}$ and $\mathbf{H} = \nabla \times \mathbf{A}$ are the electric and magnetic fields normalized by $mc^2/(ew_0)$, and $\gamma = \sqrt{1 + \mathbf{p}^2}$ is the relativistic mass factor. Eq. (11) is solved numerically below for an array of initial conditions to calculate the energy spectra of a sparse electron ensemble scattered by a relativistically intense laser field. The simulations detailed below fully take into account the three components of the electron coordinate and momentum, of the electric and magnetic field, and of the corresponding Lorentz force.

3. ELECTRON ENERGY SPECTRA FOR SPARSE TARGETS SCATTERED BY RELATIVISTICALLY INTENSE LASER PULSES

The laser radiation temporal profile adopted in the study detailed in this paper is

$$a_0(s) = ge^{-(1/2)([(s-z_d)/\tau_0])^2},$$

where τ_0 and z_d denote the laser pulse duration and the initial distance to the target, normalized respectively by w_0/c and by w_0. In the simulations described below, z_d is chosen to be large. No data accumulation over multiple laser shots is being modeled. The parameter g and the peak laser intensity I are related as $g = \sqrt{I/I_r}/\epsilon$. The simulations described below apply to targets consisting of electrons injected into the focal area or born within it due to the ionization of low-density gas by the pulse front.

Provided that the target is sufficiently sparse, the resulting electron dynamics can be modeled by solving Newton's equations for each particle independently as the Coulomb forces within it are negligible compared with the optical field Lorentz force (Galkin, 2008). Assuming that the above condition is met, which is the case for the gas density in the experimental settings described by Kalashnikov *et al.* (2015), the electron scattering is simulated in the present study by solving Eq. (11) for an array of initial conditions. The electrons are initially distributed uniformly over large target space and launched with noise-level start momenta, with no attempt being made to assign statistical weights to individual particles.

The electrons were born via the optical field ionization in the case of the study by Kalashnikov *et al.* (2015). The above approach based on treating electrons as a pre-existing environment is warranted for the simulation of the experimental conditions of the study as, for the intensity achieved in it, ionization occurs far at the front of the pulse, with the high-intensity temporally central part of the optical field running into the thus preformed electron target.

The electron energy spectra were measured under same conditions for Ar and Kr to diagnose the potential influence of the optical field ionization and proved to be practically identical (Kalashnikov *et al.*, 2015), demonstrating that the experiment for the given intensity did not extend beyond full ionization of Ar. An estimate using the Coulomb barrier suppression model (Augst *et al.*, 1989, 1991) shows that, in the case of Ar, achieving the two maximally ionized states should take the intensity of around $(4–5) \times 10^{21}$ W/cm^2, which is slightly out of reach under the experimental conditions discussed by Kalashnikov *et al.* (2015), while the third-highest ionized state only requires an intensity close to 10^{19} W/cm^2 and should materialize ahead of the advent of the high-intensity part of the laser pulse. Consequently, the major strong-field scattering action of the laser radiation occurred, under the given conditions, in an electron environment already created at the pulse rise. It should be noted that, therefore, the effect of exceptionally efficient acceleration of electrons due to their being discharged via ionization right into the focal spot, as described elsewhere (Hu & Starace, 2002, 2006), was absent. Not being injected right into the focal spot due to the above effect or to pre-acceleration, the electrons tend to be scattered by the laser pulse before the focal spot covers them, which explains the fact that the electron energies recorded in the recent experimental study (Kalashnikov *et al.*, 2015) and reproduced in computations below appear modest compared to the energy of the oscillations an electron would exhibit in a field with the amplitude corresponding to the peak laser intensity considered.

As shown in previous studies (Galkin *et al.*, 2008), an electron interacting with a focused intense laser pulse is captured by the optical field, oscillates in it, and, finally, drops out of the focal spot due to dephasing as the pulse propagating with the speed of light overtakes the accelerated particle. The focused optical field being transversely inhomogeneous,

https://doi.org/10.1017/S0263034616000823 Published online by Cambridge University Press

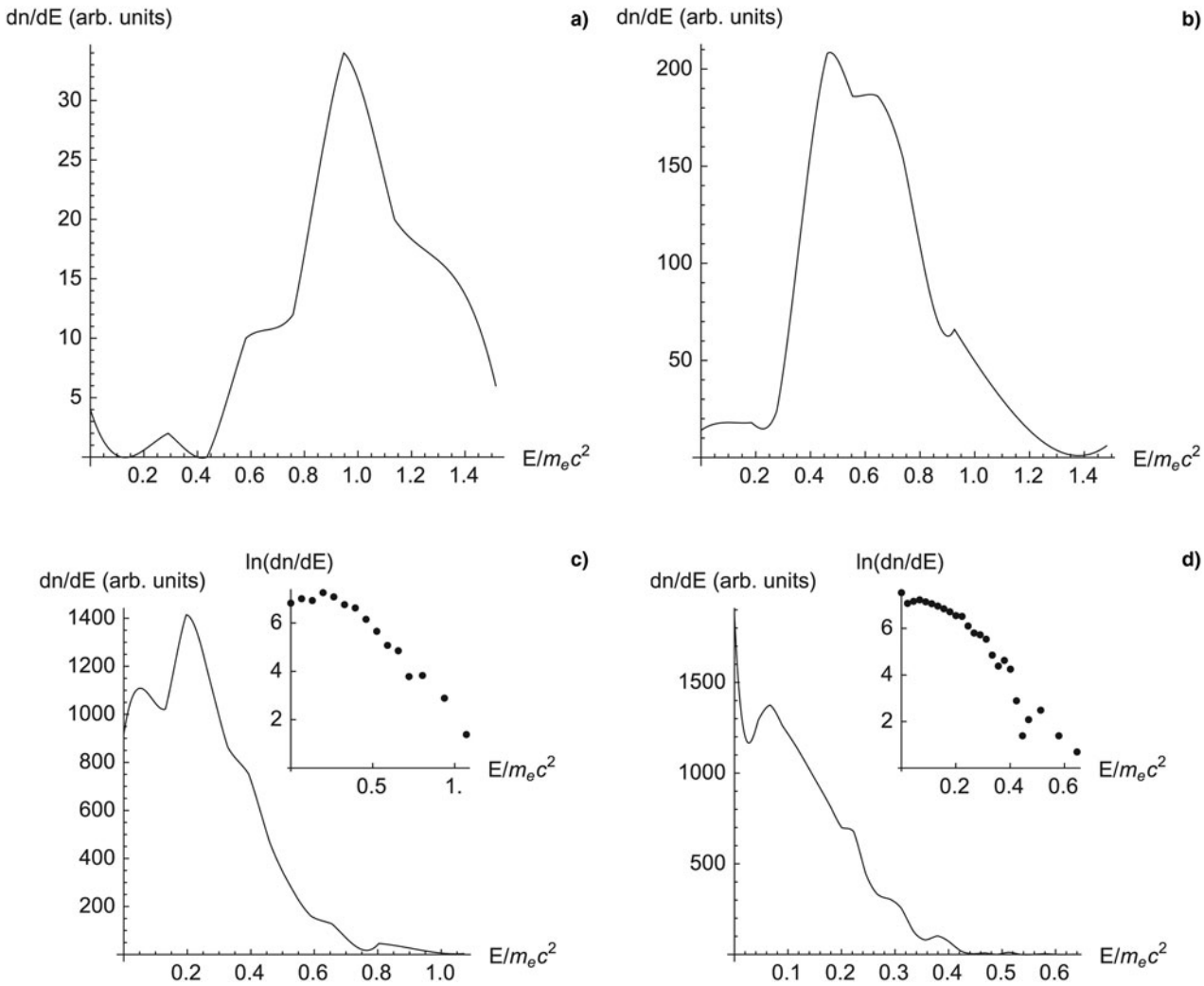

Fig. 2. The energy spectra of electrons scattered into various angular angular ranges relative to the propagation axis by a laser pulse with a Gaussian transverse distribution of amplitude and the peak intensity, duration, and focal spot radius respectively equal to $50I_r$ [where I_r stands for the relativistic intensity given by Eq. (1)], 11.24 optical cycles, and 2.75 laser wavelengths. The results are shown for the angular ranges making (a) 40°–50°; (b) 50°–60°; (c) 60°–70°; (d) 70°–80°. The spectra in (c) and (d) are also presented in insets in semi-logarithmic scale to illustrate the near-exponential character of the corresponding energy distributions.

the electron gets displaced radially relative to its original position over the interaction time and, therefore, is eventually released at an angle to the propagation axis with a kinetic energy, which can make a considerable fraction of the energy acquired in the process of laser-driven oscillations. For an electron ensemble, the outputs combine into electron energy spectra, which are recorded within various angular ranges relative to the laser pulse propagation axis.

Representative simulation results for the electron energy spectra produced by the interaction between a sparse target and relativistically intense laser radiation are shown in Figures 1 and 2. The laser pulse was assumed to have the peak intensity of $50I_r$, the duration of 11.24 optical cycles, and the focal spot radius of 2.75 laser wavelengths [roughly, these are the laser system parameters reported by Kalashnikov *et al.* (2015)]. The amplitude transverse distributions in the optical fields correspond to a Gaussian pulse in Figure 1 and to the first Laguerre mode [$l = 0$ and $\delta = 1$ in Eq. (10)] comprising a Gaussian core and a ring – in Figure 2, the purpose being to assess how the electron energy spectra are affected by the optical field transverse structure. The angular ranges for which the spectra are depicted are chosen in each case to highlight the patterns specific to the scattering induced by Gaussian and Laguerre laser pulses. The data in Figure 1 correspond to (a) 40°–50°; (b) 50°–60°; (c) 60°–70°; (d) 70°–80°, and in Figure 2 – to (a) 10°–20°; (b) 30°–40°; (c) 40°–50°. Electrons with noise-level post-interaction energies ($\leq 0.001mc^2$) were filtered out of the spectra, and the energy mesh was slightly adapted to the character of the distributions by using finer divisions to visualize the cold fringes where the numbers of particles tend to be much higher. The resultant discrete spectra were interpolated.

The key finding illustrated by Figures 1 and 2 is that significantly different patterns arise in the energy spectra of

https://doi.org/10.1017/S0263034616000823 Published online by Cambridge University Press

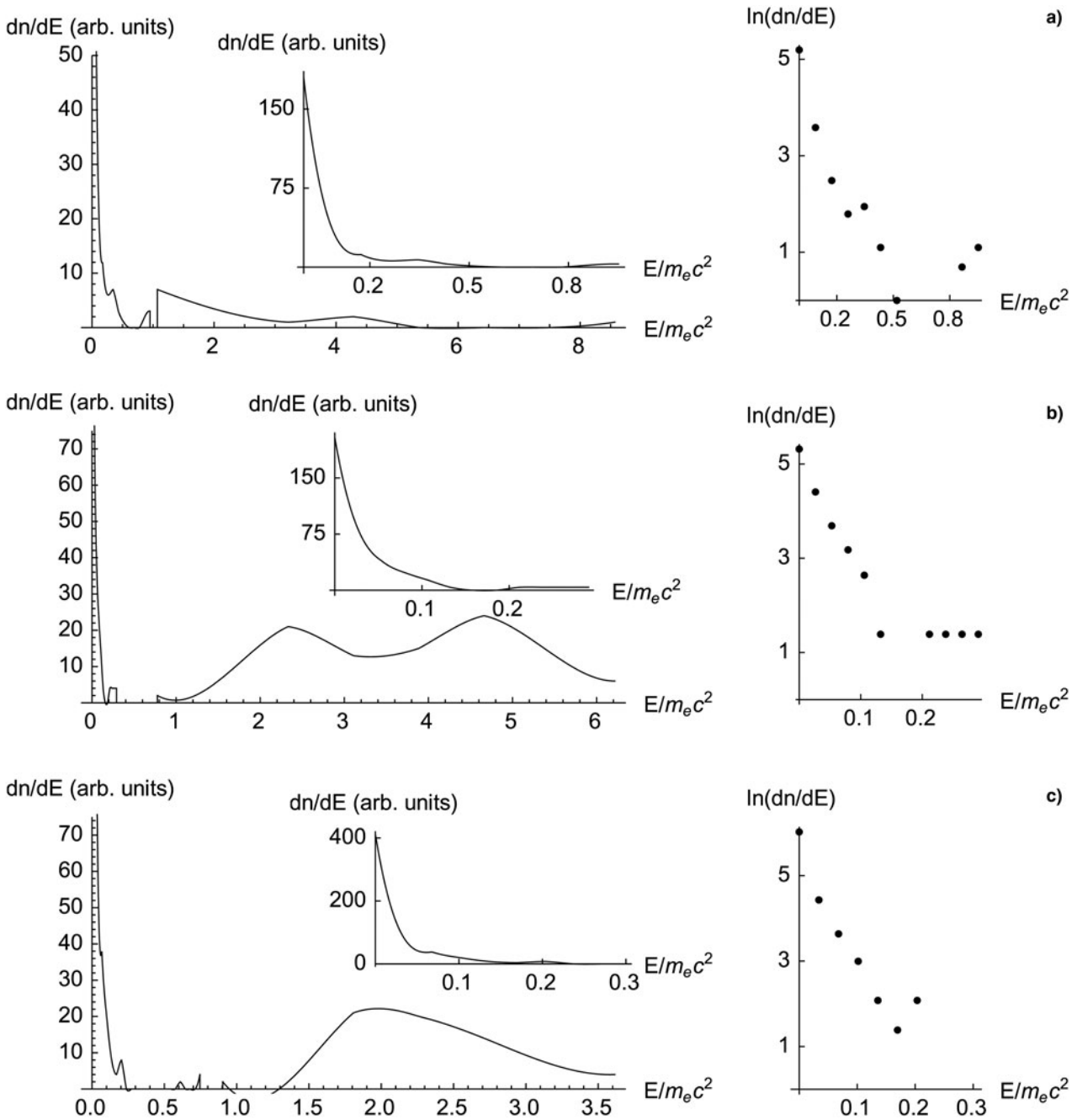

Fig. 3. The energy spectra of electrons scattered into various angular ranges relative to the propagation axis by a laser pulse with a Laguerre transverse distribution of amplitude and the peak intensity, duration, and focal spot radius respectively equal to $50I_r$ [where I_r stands for the relativistic intensity given by Eq. (1)], 11.24 optical cycles, and 2.75 laser wavelengths. The results are shown for the angular ranges making (a) 10°–20°; (b) 30°–40°; (c) 40°–50°. For every angular range, the figures include the overall spectrum with the cold part capped to accentuate the features of the relativistic component, an inset showing the cold part in full range, and a semi-logarithmic plot of the cold part illustrating its near-exponential character.

the electron ensembles scattered by relativistically intense laser pulses with Gaussian and Laguerre transverse distributions of the laser field amplitude. For a Gaussian pulse, the angular range where the maximal electron energy is attained exhibits a distribution localized around the peak value, as can be seen in Figure 2a. The localization effect holds within a neighboring angular range with a lower peak energy (Fig. 2b), but the type of behavior changes as greater deviations from the laser propagation axis are examined. For those, the energy spectra, exemplified by Figures 2c and 2d, are dominated by cold electrons and have the form of evanescent distributions. Their near-exponential character over large parts of the energy diapason is illustrated by the insets in Figures 2c and 2d showing the same data in semi-logarithmic scale.

https://doi.org/10.1017/S0263034616000823 Published online by Cambridge University Press

In a crucial contrast, the energy spectra of the electrons scattered by a Laguerre-mode laser pulse combine cold and high-energy components within many of the angular ranges. For some of them, the relativistic parts of the spectra have complex shapes, such as the twin-maxima structure visible in Figure 3b. The insets in Figures 3a–3c show uncurtailed zooms of the cold components, while their semi-logarithmic plots, which are also presented in Figure 3, attest to their exponential character.

With these patterns prominent in the scattering picture for the Laguerre-mode transverse structure of the optical field, the corresponding simulated energy spectra bear strong semblance of the experimental findings (Kalashnikov *et al.*, 2015) which are reproduced in Figures 1b and 1c. Note that the focal spot structure seen in the photo in Figure 1a, taken from the study by Kalashnikov *et al.* (2015), supports the assumption that the optical field in the case had a first-order Laguerre transverse distribution of amplitude.

Fully quantitative comparison between the experimental results (Kalashnikov *et al.*, 2015) and the above computations is problematic as the observations data underwent statistical processing in the former case and is fairly sensitive to computational parameters in the latter. Moreover, a plethora of contributing factors including the laser pulse contrast, temporal profile, and so on may not be fully taken into account. Nevertheless, there appears to be reasonable agreement between the observations and the simulation outcomes shown respectively in Figures 1b and 3b as well as between Figures 1c and 3c. In Figure 1b, the sub-relativistic part is an exponentially decreasing distribution followed by a plateau, which altogether fit within the energy range of under $0.5mc^2$, a structure similar to the one depicted in Figure 3b. The characteristic twin-peak formation in the relativistic diapason is present in both figures, with the maxima in the computational picture positioned approximately at $2.2mc^2$ and $4.6mc^2$. The values differ from the corresponding ones in Figure 1b by around $0.5mc^2$, which is considerably less than the widths of the peaks [in computations, the widths come out to be close to those observed experimentally by Kalashnikov *et al.* (2015)]. An exponential cold part somewhat wider than in the previous pair of figures is found in both Figures 1c and 3c, while the scarcely distinguishable relativistic-range peaks in Figure 1c are matched by a single pileup of relativistic electrons in the computational data given in Figure 3c. The onset of the relativistic part of the distribution in Figure 3c is also shifted in comparison with that of Figure 1c by around $0.5mc^2$, a value much less than the combined width of the peaks.

It should be noted that, overall, the shapes of the simulated energy spectra appear to be sensitive to the full number of energy scale divisions and to how the total angle is partitioned into ranges, so that the more meaningful aspects of the description of the scattering of electrons by laser pulses are reflected by the data on the widths of the energy distributions.

4. SUMMARY

The post-interaction energy spectra of electrons scattered by relativistically intense laser pulses into various ranges of angles relative to the optical field propagation axis are examined. The concentration in the electron ensemble is assumed to be low enough to neglect the Coulomb interactions between electrons as well as between electrons and the ion carcass if target ionization by the laser pulse front is implied.

The electron dynamics is modeled by treating the relativistic Newton equation for an array of initial conditions, the charged particles being driven by the Lorentz force exerted by a focused electromagnetic envelope. An approximate solution to the Maxwell equations in vacuum is spelled out to describe the envelope, with the longitudinal field and short-pulse corrections (which are of the same order) taken into account. In the general case, the solution can be represented as a series of Laguerre modes, the lowest one corresponding to the Gaussian transverse intensity distribution.

Simulation results are presented for the Gaussian mode and for the first Laguerre mode, which can be interpreted as a superposition of a Gaussian distribution and an optical field ring. The latter case appears to reproduce the features seen in the laser focus photo from a recent experimental study (Kalashnikov *et al.*, 2015).

Computations demonstrate that the electron energy spectra within particular angular ranges tend to be considerably non-monoenergetic for both Gaussian and first-order Laguerre laser pulses, but distinct patterns emerge in each case. Depending on the angular range, the spectra of the electrons ejected from the target by a Gaussian pulse either are peaked around a maximal value or have the shape of evanescent distributions stretching from the cold to the chiefly sub-relativistic zone of the spectrum. In contrast, pulses with the first-order Laguerre transverse amplitude profile produce, within certain angular ranges, grossly non-monoenergetic electron energy spectra combining cold near-exponential components and markedly relativistic parts. Furthermore, the relativistic-energy parts of the electron spectra may exhibit characteristic twin-maxima structure. Both of the above patterns emerging in the simulations for the first-order Laguerre transverse intensity distribution are recognizable in the experimentally measured electron energy spectra, which are reported by Kalashnikov *et al.* (2015).

ACKNOWLEDGMENTS

The work was partially supported in the framework of the Extreme Fields program of the Presidium of the Russian Academy of Science. The study was presented as a talk at the 34th European Conference on Laser Interaction with Matter, September 18–23, 2016, Moscow, Russia.

REFERENCES

August, S., Strickland, D., Meyerhofer, D.D., Chin, S.L. & Eberly, J.H. (1989). Tunneling ionization of noble gases

https://doi.org/10.1017/S0263034616000823 Published online by Cambridge University Press

in a high-intensity laser field. *Phys. Rev. Lett*. **63**, 2212–2215.

Augst, S., Meyerhofer, D.D., Strickland, D. & Chin, S.L. (1991). Laser ionization of noble gases by Coulomb-barrier suppression. *J. Opt. Soc. Am. B* **8**, 858–867.

Bochkarev, S.G. & Bychenkov, V.Yu. (2007). Acceleration of electrons by tightly focused femtosecond laser pulses. *Quantum Electron*. **3**, 273–284.

Borovskiy, A.V., Galkin, A.L. & Kalashnikov, M.P. (2015). Two-dimensional angular energy spectrum of electrons accelerated by the ultra-short relativistic laser pulse. *Phys. Plasmas* **22**, 043107–043107.

Bulanov, S.V., Esirkepov, T.Zh., Kando, M., Pirozhkov, A.S. & Rosanov, N.N. (2013). Relativistic mirrors in plasmas. Novel results and perspectives. *Phys. Usp*. **56**(5), 429–464.

Cao, N., Ho, Y.K., Wang, P.X., Pang, J., Kong, Q., Shao, L. & Wang, Q.S. (2002). Output features of vacuum laser acceleration. *J. Appl. Phys*. **92**, 5581–5583.

Cao, N., Ho, Y.K., Xie, Y.J., Pang, J., Chen, Z., Shao, L., Kong, Q. & Wang, Q.S. (2004). Interaction of an electron bunch with a laser pulse in vacuum. *Appl. Phys. B* **78**, 781–790.

Esarey, E., Schroeder, C.B. & Leemans, W.P. (2009). Physics of laser-driven plasma-based electron accelerators. *Rev. Mod. Phys*. **8**(1), 1229–1285.

Galkin, A.L., Korobkin, V.V., Romanovsky, M.Yu. & Shiryaev, O.B. (2010). Electrodynamics of electron in a superintense laser field: New principles of diagnostics of relativistic laser intensity. *Phys. Plasmas* **17**, 053105–053105.

Galkin, A.L., Korobkin, V.V., Romanovsky, M.Yu. & Shiryaev, O.B. (2008). Dynamics of an electron driven by relativistically intense laser radiation. *Phys. Plasmas* **15**, 023104.

Galkin, A.L., Korobkin, V.V., Romanovskiy, M.Yu., Trofimov, V.A. & Shiryaev, O.B. (2012). Acceleration of electrons to high energies in the field of a standing wave generated by counterpropagating intense laser pulses with tilted amplitude fronts. *Phys. Plasmas* **19**, 073102–073102.

Hartemann, F.V., Van Meter, J.R., Troha, A.L., Landahl, E.C., Luhmann Jr., N.C., Baldis, H.A., Gupta, A. & Kerman, A.K. (1998). Three-dimensional relativistic electron scattering in an ultrahigh-intensity laser focus. *Phys. Rev. E* **58**, 5001–5012.

Hua, J.F., Ho, Y.K., Lin, Y.Z., Chen, Z., Xie, Y.J., Zhang, S.Y., Yan, Z. & Xu, J.J. (2004). High-order corrected fields of ultrashort, tightly focused laser pulses. *Appl. Phys. Lett*. **85**, 3705–3707.

Hu, S.X. & Starace, A.F. (2002). GeV electrons from ultraintense laser interaction with highly charged ions. *Phys. Rev. Lett*. **88**, 245003–245003.

Hu, S.X. & Starace, A.F. (2006). Laser acceleration of electrons to giga-electron-volt energies using highly charged ions. *Phys. Rev. E* **73**, 066502.

Kalashnikov, M., Andreev, A., Ivanov, K., Galkin, A., Korobkin, V., Romanovsky, M., Shiryaev, O., Schnuerer, M., Braenzel, J. & Trofimov, V. (2015). Diagnostics of peak laser intensity based on the measurement of energy of electrons emitted from laser focal region. *Laser Part. Beams* **33**, 361–366.

Kong, Q., Ho, Y.K., Wang, J.X., Wang, P.X., Feng, L. & Yuan, Z.S. (2000). Conditions for electron capture by an ultraintense stationary laser beam. *Phys. Rev. E* **61**, 1981–1984.

Korobkin, V.V., Romanovskiy, M.Yu., Trofimov, V.A. & Shiryaev, O.B. (2013). Concept of generation of extremely compressed high-energy electron bunches in several interfering intense laser pulses with tilted amplitude fronts. *Laser Part. Beams* **31**, 23–28.

Li, J.-X., Zang, W.-P. & Tian, J.-G. (2010). Vacuum laser-driven acceleration by Airy beams. *Opt. Express* **18**(7), 7300–7306.

Malka, V. (2012). Laser plasma accelerators. *Phys. Plasmas* **19**, 055501–055501.

Mori, W.B. (2007). The development of laser- and beam-driven plasma accelerators as an experimental field. *Phys. Plasmas* **14**, 055501–055501.

Mourou, G.A., Tajima, T. & Bulanov, S.V. (2006). Optics in the relativistic regime. *Rev. Mod. Phys*. **78**, 309–371.

Norreys, P.A., Beg, F.N., Sentoku, Y., Silva, L.O., Smith, R.A. & Trines, R.M.G.M. (2009). Intense laser-plasma interactions: New frontiers in high energy density physics. *Phys. Plasmas* **16**, 041002–041002.

Ohkubo, T., Bulanov, S.V., Zhidkov, A.G., Esirkepov, T., Koga, J., Uesaka, M. & Tajima, T. (2006). Wave-breaking injection of electrons to a laser wake field in plasma channels at the strong focusing regime. *Phys. Plasmas* **13**, 103101–103101.

Pang, J., Ho, Y.K., Yuan, X.Q., Cao, N., Kong, Q., Wang, P.X., Shao, L., Esarey, E.H. & Sessler, A.M. (2002). Subluminous phase velocity of a focused laser beam and vacuum laser acceleration. *Phys. Rev. E* **66**, 066501–066501.

Payeur, S., Fourmaux, S., Schmidt, B.E., MacLean, J.P., Tchervenkov, C., Légaré, F., Piché, M. & Kieffer, J.C. (2012). Generation of a beam of fast electrons by tightly focusing a radially polarized ultrashort laser pulse. *Appl. Phys. Lett*. **101**, 041105–041105.

Quesnel, B. & Mora, P. (1998). Theory and simulation of the interaction of ultraintense laser pulses with electrons in vacuum. *Phys. Rev. E* **58**, 3719–3732.

Salamin, Y.I., Mocken, G.R. & Keitel, C.H. (2002). Electron scattering and acceleration by a tightly focused laser beam. *Phys. Rev. E ST - Accel. Beams* **5**, 101301–101301.

Wang, J.X., Ho, Y.K., Kong, Q., Zhu, L.J., Feng, L., Scheid, S. & Hora, H. (1998). Electron capture and violent acceleration by an extra-intense laser beam. *Phys. Rev. E* **58**, 6575–6577.

Wang, P.X., Ho, Y.K., Yuan, X.Q., Kong, Q., Cao, N., Sessler, A.M., Esarey, E. & Nishida, Y. (2001). Vacuum electron acceleration by an intense laser. *Appl. Phys. Lett*. **78**, 2253–2255.

Wang, J.X., Ho, Y.K., Kong, Q., Zhu, L.J., Feng, L., Scheid, S. & Hora, H. (2002). Characteristics of laser-driven electron acceleration in vacuum. *J. Appl. Phys*. **91**, 856–866.

Wang, P.X., Ho, Y.K., Tang, Ch.X. & Wang, W. (2007). Field structure and electron acceleration in a laser beam of a high-order Hermite-Gaussian mode. *J. Appl. Phys*. **101**, 083113–083113.

Zheng, L., Wang, P.X., Chen, Z., Kong, Q., Ho, Y.K. & Kawata, S. (2008). Optimum injection momentum for electrons in vacuum laser acceleration. *Europhys. Lett*. **82**, 64001–64001.